Enhanced tunneling electroresistance effect by designing interfacial ferroelectric polarization in multiferroic tunnel junctions

L. N. Jiang [1], Yun-Peng Wang,[2] Y. Zhu,[1] and X. F. Han [1,3,4,*]

[1]*Beijing National Laboratory for Condensed Matter Physics, Institute of Physics, Chinese Academy of Sciences, Beijing 100190, China*

[2]*School of Physics and Electronics, Hunan Key Laboratory for Super-micro Structure and Ultrafast Process, Central South University, Changsha 410083, China*

[3]*Center of Materials Science and Optoelectronics Engineering, University of Chinese Academy of Sciences, Beijing 100049, China*

[4]*Songshan Lake Materials Laboratory, Dongguan, Guangdong 523808, China*

(Received 6 September 2021; revised 6 January 2022; accepted 28 March 2022; published 11 April 2022)

Due to the long electrical screening length of an insulator, changes in local ferroelectric (FE) polarization can cause significant electrostatic potential drops or rises across the whole insulating region, which can be designed to enhance the tunneling electroresistance (TER) effect. First-principles calculations of $Co_2MnSi/BaTiO_3/SrRuO_3$ multiferroic tunnel junctions predict a unique local FE polarization at the MnSi-TiO_2 interface, which is giant (tiny) in the right-polarized (left-polarized) state. For the right-polarized state, the large interfacial FE polarization greatly lowers the FE barrier height, making it close to zero. However, for the left-polarized state, because its band edges near the MnSi-TiO_2 interface are usually below the Fermi level, the tiny interfacial FE polarization has a weak effect on the electrostatic potential, maintaining a sizable barrier height. This FE-controlled barrier height produces an optimistic TER ratio of up to 1.1×10^3. Even if the large interface polarization is unexpectedly fixed, the TER ratio remains ultrahigh, increasing the fault tolerance of the interface-enhanced TER effect in applications.

DOI: 10.1103/PhysRevB.105.134410

I. INTRODUCTION

Both the multiferroic tunnel junction (MFTJ), with a "ferromagnetic (FM) electrode/ferroelectric (FE) barrier/FM electrode" structure, and the ferroelectric tunnel junction (FTJ), with a "metal electrode/FE barrier/metal electrode" structure, have attracted much attention over the past decade, owing to their rich physics in nanoelectronics and their potential value in data storage [1–4]. With the reversal of the FE polarization direction in the barrier, the effective barrier height or width of a tunnel junction with inversion symmetry breaking will be changed, thus presenting two different resistance values [5,6]. Such a tunneling electroresistance (TER) effect is a key property of MFTJs and FTJs. For the application of MFTJs and FTJs in electronic devices, we need a sizable and reproducible TER effect.

In general, a high TER effect can be obtained by distinct screening lengths at either side of the FE barrier [6–9], such as a $SrRuO_3/SrTiO_3/BaTiO_3$ (BTO)$/SrRuO_3$ junction with unequal screening lengths of $SrRuO_3$ and $SrTiO_3$ [6]. By designing the two sides of the FE barrier as metal (short screening length) and insulator (long screening length), an ultrahigh TER ratio can be obtained.

In our previous work, we reveal an interface-enhanced TER effect [10]. A large FE displacement at one interface of tunnel junctions will cause a significant band offset, and the direction of the interfacial FE polarization determines whether the band moves upward or downward [10]. By electrically switching the FE polarization direction, the magnitude and the direction of the large interfacial FE polarization can be modulated, leading to an ultrahigh TER effect. However, the predicted Co-$(TiO_2$-$BaO)_N$-Co junction is hard to prepare experimentally. Moreover, at present, the interface of the tunnel junction is fragile and difficult to control with precision. In practical applications, the tunnel junction may develop defects or a "dead layer" at this interface, which may be accompanied by uncontrollable large interfacial FE displacement.

In this work, taking a $Co_2MnSi/BTO/SrRuO_3$ MFTJ with a MnSi-TiO_2 termination as an example, we demonstrate via first-principles calculation that the TER effect can be significantly enhanced by designing the terminal structures to affect the interfacial FE polarization. At the MnSi-TiO_2 interface, the buckling of the O atom caused by different bond lengths of Mn-O and Si-O immensely increases (decreases) the interfacial FE polarization of the right-polarized (left-polarized) state. In the right-polarized (left-polarized) system, because the conduction band minimum is normally above (below) the Fermi level near the MnSi-TiO_2 interface, the unique interface polarization has a giant (tiny) influence on the barrier height. The TER ratio produced by the interface-enhanced principle is as high as 1.1×10^3. Even if we artificially fix the large interface polarization, the MFTJ still presents a colossal TER ratio, indicating a stable interface-enhanced TER effect.

II. COMPUTATIONAL METHOD

Calculations of atomic and electronic structures are performed by the Vienna *ab-initio* simulation package (VASP) [11] using density function theory (DFT). The exchange and

*Corresponding author: xfhan@iphy.ac.cn

correlation potential is PBEsol [12], which is a modified Perdew-Burke-Ernzerhof generalized gradient approximation (GGA) and designed specifically for solids. We use the projector augmented wave pseudopotential [13,14], under the limitation of a 500-eV cutoff energy. Because the thin BTO barrier in the $Co_2MnSi/BTO/SrRuO_3$ MFTJ with a MnSi-TiO_2 termination cannot maintain spontaneous FE polarization, we use a relatively thick BTO barrier with 10 unit cells (about 4 nm). The slab for the $Co_2MnSi/BTO/SrRuO_3$ junction along [001] consists of 9 monolayers (MLs) of Co_2MnSi (>1 nm), 20 MLs of BTO (about 4 nm), 8 MLs of $SrRuO_3$ (>1 nm), and a 15-Å-thick vacuum to separate the periodic slabs. The in-plane lattice constant is fixed to 3.905 Å, in order to simulate the epitaxial growth on a commonly used $SrTiO_3$ substrate. The lattice mismatch is about 2% for Co_2MnSi ($5.64/\sqrt{2}$ Å), 2% for BTO (3.99 Å), and 0.6% for $SrRuO_3$ (3.93 Å). Under the in-plane constraint, we relax the whole structure until the force on each atom is less than 0.01 eV/Å. For the Brillouin-zone sampling, we use a $7 \times 7 \times 1$ Gamma mesh for relaxation calculations, $13 \times 13 \times 1$ for self-consistent calculations, and $15 \times 15 \times 1$ for density-of-states (DOS) calculations, corresponding to the Gaussian smearing of 0.1, 0.05, and 0.05 eV, respectively. The energy convergence criterium is set to 1×10^{-5} eV. In addition, since the $Co_2MnSi/BTO/SrRuO_3$/vacuum is an asymmetric slab, we also considered the dipole correction for relaxation, self-consistent, and DOS calculations. Comparing the results with and without dipole correction, we find that dipole correction has little effect on this study.

The transport calculations are performed using NANODCAL [15], which combines the DFT with the Keldysh nonequilibrium Green's function (NEGF) formalism. The $\mathbf{k}_{\parallel}$ mesh of self-consistent calculation is 13×13 for the MnSi-TiO_2 terminated MFTJ and 12×12 for the fixed MnSi-TiO_2 terminated MFTJ. For the calculations of conductance, due to the existence of some hot spots in the two-dimensional Brillouin zone (2DBZ), we take different points in different areas. The number of sampling points is between 300×300 and 1000×1000. We take more points at some small areas with fast changes and take fewer points at regions with gentle changes. The final change of conductance is stable within 5% under the increase of sampling points.

III. RESULTS AND DISCUSSION

To model the system with a special interfacial FE polarization, we consider a $Co_2MnSi/BTO/SrRuO_3$ tunnel junction whose two terminations are MnSi-TiO_2 and BaO-RuO_2. BTO is a typical perovskite FE material with spontaneous polarization and a high Curie temperature. The magnetic metal $SrRuO_3$ with perovskite structure is prone to form epitaxial structures with other perovskite materials and can be experimentally prepared together with BTO as $SrRuO_3$/BTO heterostructures with an atomically sharp interface [16]. The Co_2MnSi electrode is a half-metallic ferromagnet with a spin polarization theoretically close to 100%. In this study, the Co_2MnSi electrode is mainly used to obtain a special interfacial FE polarization at the MnSi-TiO_2 termination [17] to modulate the TER effect. Moreover, the stability phase diagram of the Co_2MnSi-BTO [18] interface indicates that

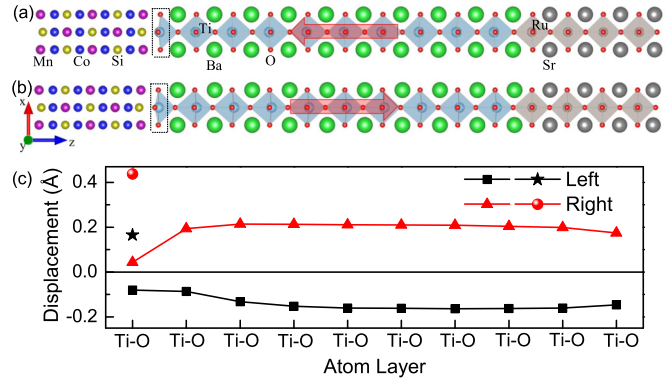

FIG. 1. Relaxed structures of (a) left-polarized and (b) right-polarized $Co_2MnSi/BTO/SrRuO_3$ MFTJs with the MnSi-TiO_2 termination. Red arrows in BTO indicate the FE polarization directions. The black dotted frames in panels (a) and (b) indicate the special Ti-O layer. (c) Ti-O displacements in left-polarized (black square) and right-polarized (red triangle) BTO. The special Ti-O_{Si} displacement at the MnSi-TiO_2 interface is marked with a black star (left polarization) and a red ball (right polarization).

the MnSi-TiO_2 termination is stable under Mn-rich and Co-poor conditions. We also calculated the separation energy of the MnSi-TiO_2 interface, which is positive in both the left-polarized state (1.587 J/m^2) and the right-polarized state (2.376 J/m^2). Furthermore, a similar FeSi-TiO_2 termination in the $Co_2FeSi/SrTiO_3$ system has been successfully prepared in experiment [19]. Co_2MnSi and BTO have structures and lattice constants similar to those of Co_2FeSi and $SrTiO_3$, respectively. Accordingly, this study considers the $Co_2MnSi/BTO/SrRuO_3$ MFTJ not only because it is likely to demonstrate our research goal but also because the structure is expected to be experimentally realized.

The relaxed structures of the $Co_2MnSi/BTO/SrRuO_3$ MFTJs with a MnSi-TiO_2 termination are shown in Figs. 1(a) and 1(b). FE polarization pointing from Co_2MnSi to $SrRuO_3$ (from $SrRuO_3$ to Co_2MnSi) is defined as the right-polarized (left-polarized) state. The relative displacement along the z direction for each TiO_2 layer is shown in Fig. 1(c). Usually, the Ti-O displacement is relatively uniform and slightly reduced at the interface [20–22]. However, a unique FE displacement occurs at the MnSi-TiO_2 interface. We define the O atom on top of the Mn (Si) atom at this interface as O_{Mn} (O_{Si}). The Ti-O_{Mn} displacement is only about −0.08 Å (0.04 Å) in the left (right) polarization. The Ti-O_{Si} displacement of the right-polarized state indicated by the red ball in Fig. 1(c) is as large as 0.44 Å. After averaging with Ti-O_{Mn} displacement, it is about 0.24 Å. Polarization (P) can be roughly expressed by the Ti-O displacement δ_z as $P = 20\ Cm^{-2}\ nm^{-1}\ \delta_z$ [4]. The interfacial FE polarization is estimated to be 0.48 Cm^{-2}, representing a large polarization for BTO. The Ti-O_{Si} displacement of the left-polarized state marked with the black star in Fig. 1(c) is 0.17 Å, which is opposite to the direction of the left-polarized bulk. After averaging with the Ti-O_{Mn} displacement, it is about 0.05 Å and the corresponding polarization is 0.10 Cm^{-2}.

The unique FE displacements at the MnSi-TiO_2 interface originate from the difference between the Mn-O bond length

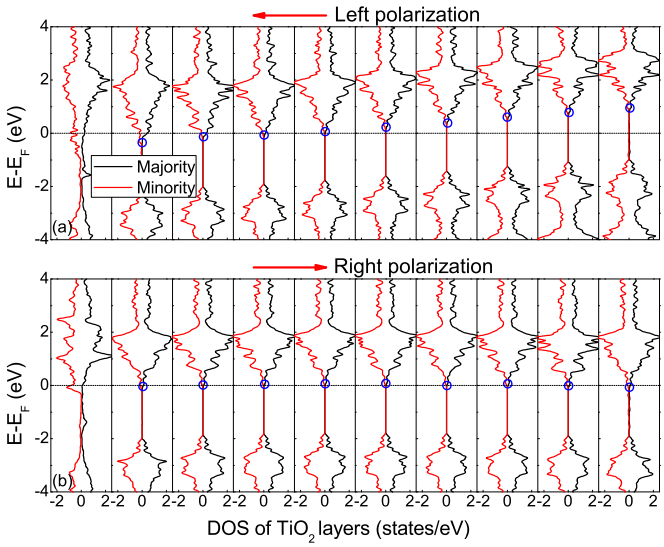

FIG. 2. Spin-resolved DOS on the TiO_2 layer in (a) left-polarized and (b) right-polarized $Co_2MnSi/BTO/SrRuO_3$ MFTJs with a MnSi-TiO_2 termination. Black (red) lines represent the majority-spin (minority-spin) DOS. From the left to the right, the DOS diagrams correspond to the TiO_2 layer from the MnSi-TiO_2 interface to near the BaO-RuO_2 interface. The CBM is indicated by blue circles.

and the Si-O bond length. The Mn-O bond length is longer than the Si-O bond length, due to the larger radius of the Mn atom than the Si atom. In the left-polarized case, the Mn-O and Si-O bond lengths are about 1.92 and 1.82 Å, respectively. The corresponding values for the right-polarized case are 1.96 and 1.77 Å, respectively. This restricts the spontaneous FE polarization of the BTO barrier when the bonding energy at the MnSi-TiO_2 interface can overcome the ferroelectricity of BTO [17]. The resulting O atom buckling makes the FE polarization at the MnSi-TiO_2 interface tend to point away from the interface, promoting the right-polarized state (with a large interface displacement) and weakening the left-polarized state (with a right-polarized interface).

As we studied earlier, the magnitude and the direction of interfacial FE polarization can modulate the energy band of the FE barrier [10]. When the interfacial polarization direction points to (away from) the interface, the larger the interfacial polarization is, the more the energy band of the insulating region moves upward (downward) [10]. Under the premise that the Fermi level is in the band gap, due to the long electrical screening length, the changes of local FE polarization can produce two effects in tunnel junctions: the band offset of the whole insulating region [23] and the change of the screening field. The former makes the whole band edge shift to a higher- or lower-energy position (a translation variation), and the latter changes the slope of the band edges (a rotation variation). Therefore, the unique FE displacements at the MnSi-TiO_2 interface will produce a special effect on the energy band of BTO.

To reveal the specific effects of polarization switching on the energy band of the tunnel junction, we calculate the DOS of the left- and right-polarized MFTJs, as shown in Fig. 2. The DOS of BaO layers is not shown here because their states are far from the Fermi level and hardly affect the band edges. For the left polarization [Fig. 2(a)], compared with the ordinary left-polarized interface, its unique right-polarized MnSi-TiO_2 interface tends to produce an electrostatic potential drop [10]. However, the MnSi-TiO_2 interface is generally the lowest point of the band edges in the left-polarized case and has a conduction band minimum (CBM) close to or even below the Fermi level. The interfacial electrostatic potential drop is almost completely screened by free electrons near the MnSi-TiO_2 interface, making it difficult for the special interfacial polarization to affect the whole barrier height or width. Therefore, the CBM of most of the left-polarized BTO region is above the Fermi level, presenting a conventional insulating state. For the right polarization [Fig. 2(b)], compared with the relatively small interface polarization in normal cases, the large FE polarization at the MnSi-TiO_2 interface produces a huge electrostatic potential drop, making the energy band of the BTO barrier undergo a giant downward movement. Moreover, the slope of band edges becomes a little flat, because the depolarization field of the noninterfacial layer is reduced due to the larger screening field induced by the large interfacial FE polarization. The right-polarized MFTJ finally presents a barrier height of zero in the GGA calculation. The giant difference in barrier height and width between left- and right-polarized states can qualitatively lead to a colossal TER ratio.

The GGA calculation usually underestimates the band gap of the insulator. To illustrate that the increase of the band gap will not affect the predicted tunnel junction too much, we also perform the GGA + U calculation. The Hubbard parameters on the Ru-d state are fixed to $U = 0.6$ eV and $J = 0$ eV [24]. The parameters on the Co-d and Mn-d states are both fixed to $U = 3$ eV and $J = 0.9$ eV [25]. The J value on Ti-d and Ba-d states of BTO is fixed to 0 eV, while the U value increases from 0 to 6. Part of the calculated data are included in the Appendix. As the U value on Ti-d and Ba-d states increases from 0 to 6, the band gap of BTO increases from ∼1.7 to ∼2.5 eV. The height of the left-polarized barrier becomes higher with the increasing band gap. The CBM of the right-polarized barrier is slightly altered by the increase of the band gap, but it is still near the Fermi level, presenting a barrier height close to zero. Therefore, a higher TER ratio will be obtained when the band gap increases appropriately. When the band gap increases to 3.2 eV (the experimental band gap of BTO), the barrier height of ∼2 unit cells may no longer be zero, but this happens to be favorable for the electric field regulation of the right-polarized state.

Besides, since the right-polarized BTO with zero barrier height originates from the unique FE displacement at the MnSi-TiO_2 interface, the insulation of the BTO barrier will recover when this special Ti-O displacement is modified. For this purpose, we did two tests. In the first test, we constrained the interfacial Ti-O_{Si} displacement to different values and relaxed the right-polarized MFTJ with a MnSi-TiO_2 termination under this constraint. We reduced the Ti-O_{Si} displacement from its equilibrium value of 0.44 Å to as small as 0.10 Å. With the decreasing of the Ti-O_{Si} displacement, we observed the transition of the BTO barrier from zero barrier height to insulation in the GGA calculation. This further confirms the giant modulation of the energy band by the interfacial FE polarization. In the second test, for comparison with the MnSi-

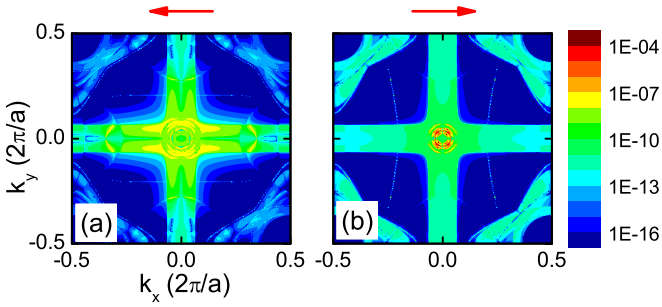

FIG. 3. The $k_{\|}$-resolved transmission distributions at the Fermi energy in the 2DBZ for tunnel junctions with MnSi-TiO_2 termination. Panels (a) and (b) are the left-polarized case and the right-polarized case, respectively.

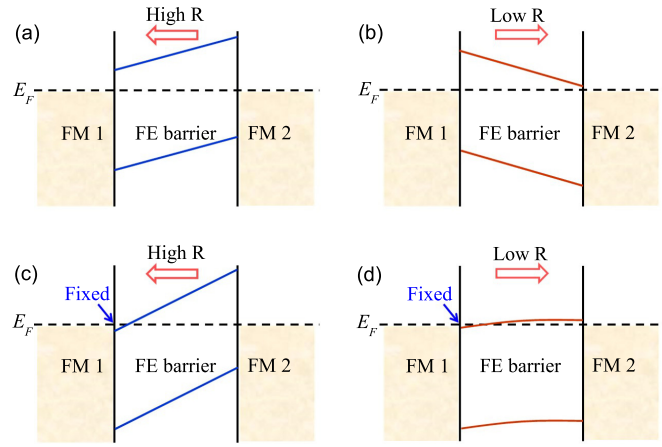

FIG. 4. TER effect diagrams of (a), (b) typical MFTJs and (c), (d) interface-fixed MFTJs. The fixed interface with a pinned and large interfacial FE polarization pointing away from the interface is marked with blue arrows in panels (c) and (d). Red arrows indicate the FE polarization direction.

TiO_2 termination, we consider the Co_2MnSi/BTO/$SrRuO_3$ junction with a Co_2-TiO_2 termination (see the Appendix). The Ti-O displacement at the Co_2-TiO_2 interface is -0.10 (0.14) Å in the left-polarized (right-polarized) case. With such a normal interfacial FE polarization, the BTO barrier presents conventional insulating states in both left and right polarization. This once again proves the importance of the unique FE displacement at the MnSi-TiO_2 interface.

Following the above qualitative analysis, we further carried out the quantum transport calculations. Figure 3 shows the $k_{\|}$-resolved transmission coefficients at the Fermi energy in the 2DBZ. The MnSi-TiO_2 terminated tunnel junction with two polarized states shows similar shape of transmission distributions in 2DBZ. The symmetry of the transmission distribution is C_{2v}, which is consistent with the lattice symmetry. The main difference is around the Γ ($k_x = k_y = 0$) point, where many hot spots appear in the right-polarized state. These hot spots that form circles around the Γ point [Fig. 3(b)] are similar to the transmission shape of electron-doped BTO [26], which greatly improves the tunneling probability. They should originate from the overlap of the CBM with the Fermi level in the right-polarized MFTJ [Fig. 2(b)]. When the two FM electrodes are fixed in a parallel configuration, the calculated conductance and the TER ratio for tunnel junctions with distinct terminations are shown in Table I. The conductance of the right-polarized MnSi-TiO_2 terminated structure (8.1×10^{-7}) is several orders of magnitude higher than that of the left-polarized case (7.3×10^{-10}). The optimistic TER ratio is defined as TER $= (G_{\rightarrow} - G_{\leftarrow})/G_{\leftarrow}$, with $G_{\leftarrow}$ ($G_{\rightarrow}$) being the total conductance for the left-polarized (right-polarized) case. It is about 1.1×10^3 for the studied tunnel junction.

TABLE I. Conductance and TER ratio for Co_2MnSi/BTO/$SrRuO_3$ MFTJs with distinct terminations. $G_{\leftarrow}$ and $G_{\rightarrow}$ are the conductance (in units of e^2/h) in the left ($\leftarrow$) polarization and the right ($\rightarrow$) polarization, respectively. The magnetic configurations of the two FM electrodes are fixed in a parallel configuration.

Termination	$G_{\leftarrow}$	$G_{\rightarrow}$	TER
Co_2-TiO_2	1.5×10^{-12}	3.0×10^{-12}	1.0
MnSi-TiO_2	7.3×10^{-10}	8.1×10^{-7}	1.1×10^3
Pinned	2.4×10^{-10}	8.1×10^{-7}	3.4×10^3

In addition to the above tunnel junction with a size-adjustable MnSi-TiO_2 interface, the Co_2MnSi/BTO/$SrRuO_3$ MFTJ with a pinned MnSi-TiO_2 interface can also enhance the TER effect. Figure 4 schematically shows the variation of effective barrier height and width with a fixed large interfacial FE polarization at one interface. The band edge of the FE barrier is usually oblique and decreases along the polarization direction, as shown in Figs. 4(a) and 4(b). It is noteworthy that the left interface is generally the lowest and the highest point of the band edges in the left-polarized case and the right-polarized case, respectively. Therefore, when a large interfacial FE polarization with direction pointing away from the left interface is fixed, it will have different effects on left and right polarization, including both electrostatic potential drop and slope of band edges, as seen from Figs. 4(c) and 4(d). On the one hand, it significantly (slightly) reduced the electrostatic potential of right (left) polarization; on the other hand, it increased (decreased) the screening field of right (left) polarization and made the band edges more flat (inclined). Therefore, a pinned key interface may still enhance the TER effect.

To simulate a pinned large interface polarization, we artificially fix a 0.44-Å Ti-O_{Si} displacement at the MnSi-TiO_2 interface, and then we calculate the changes of band edges. Because the left-polarized Co_2MnSi/BTO_{10}/$SrRuO_3$ system with a large right-polarized FE displacement at the MnSi-TiO_2 interface cannot be obtained by relaxation, we only carried out static calculations in this test. Results show that the left-polarized FE barrier still presents an insulating state, while the right-polarized state has a barrier height close to zero. Therefore, even though the large interface polarization is pinned, it can still cause giant transition in the barrier, inducing a huge TER effect. As shown in Table I, the estimated optimistic TER ratio is still as high as 3.4×10^3. Since it is an artificially pinned structure without relaxation, the value of 3.4×10^3 may not fully reflect the real situation. It is for

reference only. In general, the quantitative transport analysis gave results consistent with the qualitative analysis.

IV. SUMMARY

Via first-principles calculations of $Co_2MnSi/BTO_{10}/SrRuO_3$ MFTJs, we demonstrate an ultrahigh TER effect enhanced by interface engineering. Even if the interface is unfortunately fixed, the fixed large interface polarization may still be used to produce a considerable TER ratio. This can meet the demand for a high and stable TER effect in information storage applications of MFTJs. Furthermore, although the FM Co_2MnSi and $SrRuO_3$ electrodes are used in this study, the predicted mechanism is not limited to the FM/FE/FM MFTJ. We replaced the Co_2MnSi with a nonmagnetic metal, Al, and then relaxed the Al-BTO-$SrRuO_3$ tunnel junction with an Al-BaO termination. The Al-BaO termination presents a large interfacial Ba-O displacement at one polarized state, which also greatly modulates the barrier band and enhances the TER effect. Therefore, the interface-enhanced TER effect can be obtained in both FM/FE/FM MFTJs and metal/FE/metal FTJs.

ACKNOWLEDGMENTS

This work was supported by the National Key Research and Development Program of China (MOST, Grant No. 2017YFA0206200), the National Natural Science Foundation of China (NSFC, Grants No. 12134017, No. 51831012, No. 12061131012, and No. 12004439), and the Beijing Natural Science Foundation (Grant No. Z201100004220006) and was partially supported by the Strategic Priority Research Program (B) (Grant No. XDB33000000). The atomic structure visualization was produced with VESTA software [27]. The work was carried out at the National Supercomputer Center in Tianjin, and the calculations were performed on TianHe-1 (A).

APPENDIX

1. GGA + U results

The GGA calculation usually underestimates the band gap of the insulators, which may affect the predicted results. To exclude this factor, Figs. 5 and 6 show the results of GGA $+U$ in the $Co_2MnSi/BTO/SrRuO_3$ MFTJs with a MnSi-TiO_2 termination. The Hubbard parameters are applied to the Ru-d, Co-d, Mn-d, Ti-d and Ba-d states as described in the main text. As the U values for Ti-d and Ba-d states increase from 2 (Fig. 5) to 6 eV (Fig. 6), the band gap of BTO increases. With the increasing band gap, the height of the left-polarized barrier becomes higher, while the CBM of the right-polarized barrier is slightly altered and still near the Fermi level. Therefore, even if the band gap is increased, we can also obtain a high TER ratio in the MFTJ with a MnSi-TiO_2 termination.

2. Co_2-TiO_2 terminated MFTJ for comparison

For comparison with the MnSi-TiO_2 termination, we also consider a Co_2-TiO_2 termination. The relaxed tunnel junctions with left- and right-polarized states are presented in Figs. 7(a) and 7(b), respectively. As can be seen from Fig. 7(c), the Ti-O displacements of the two polarized states are relatively uniform and slightly reduced at the two interfaces, in accordance with Refs. [20–22].

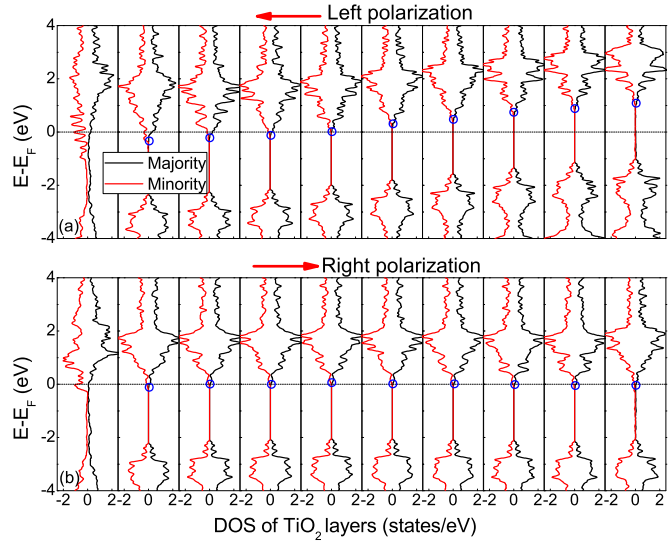

FIG. 5. Spin-resolved DOS calculated by GGA + U (U = 2 eV for Ti-d and Ba-d) for the TiO_2 layer in (a) left- and (b) right-polarized $Co_2MnSi/BTO/SrRuO_3$ MFTJs with a MnSi-TiO_2 termination. The black (red) line represents the majority-spin (minority-spin) DOS. The CBM is indicated by blue circles.

The calculated DOS of left- and right-polarized $Co_2MnSi/BTO/SrRuO_3$ MFTJs with a Co_2-TiO_2 termination are shown in Fig. 8. For both the left and the right polarization, the conduction bands of most of the BTO region are above the Fermi level, presenting a conventional insulating state. These two polarized states differ slightly in barrier height.

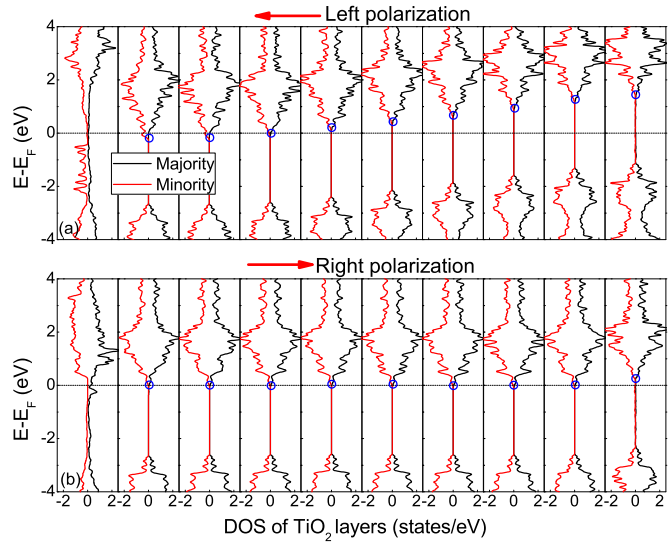

FIG. 6. Spin-resolved DOS calculated by GGA + U (U = 6 eV for Ti-d and Ba-d) for the TiO_2 layer in (a) left- and (b) right-polarized $Co_2MnSi/BTO/SrRuO_3$ MFTJs with a MnSi-TiO_2 termination. The black (red) line represents the majority-spin (minority-spin) DOS. The CBM is indicated by blue circles.

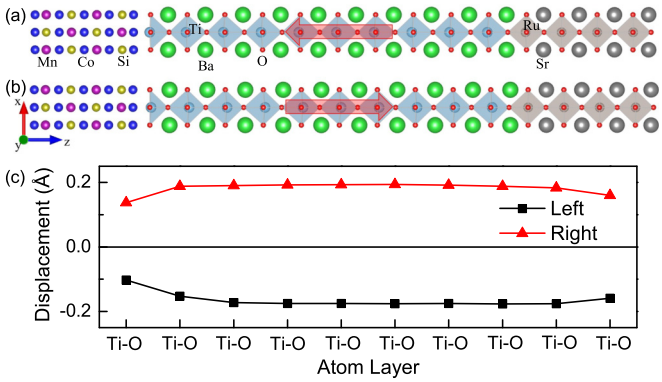

FIG. 7. Relaxed structures of (a) left-polarized and (b) right-polarized $Co_2MnSi/BTO/SrRuO_3$ MFTJs with a Co_2-TiO_2 termination. Red arrows on BTO indicate the FE polarization direction. (c) Ti-O displacements in left-polarized (black squares) and right-polarized (red triangles) BTO.

Qualitatively, this small difference leads to a modest TER ratio.

The transmission distributions of the Co_2-TiO_2 terminated system are presented in Fig. 9. The symmetry is also C_{2v}, which is consistent with the lattice symmetry. There is little difference in transmission distributions between the two polarized states, suggestive of a small TER effect. When the two FM electrodes are fixed in a parallel configuration, the calculated conductance of the right-polarized state (3.0×10^{-12}) is close to that of the left-polarized case (1.5×10^{-12}). The optimistic TER ratio is only about 1.0. The small TER effect also illustrates that the screening-length principle plays a minor role in $Co_2MnSi/BTO/SrRuO_3$ MFTJs. And the ultrahigh TER effect in the MnSi-TiO_2 terminated $Co_2MnSi/BTO/SrRuO_3$ MFTJ in the main text originates from the interface-enhancement method.

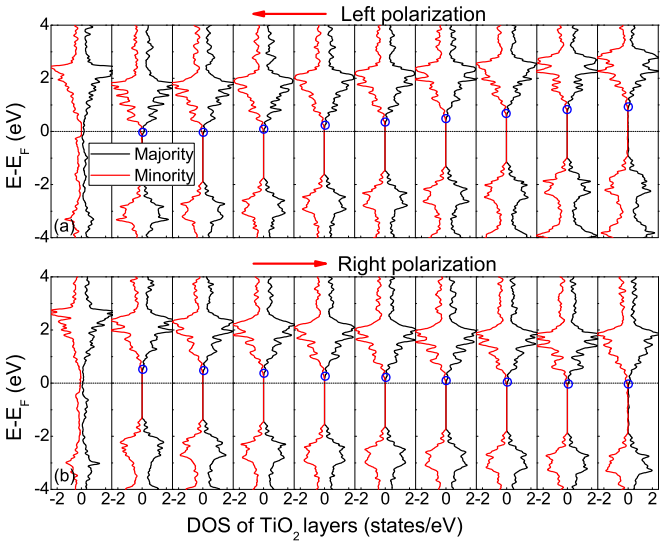

FIG. 8. Spin-resolved DOS on TiO_2 layer in (a) left- and (b) right-polarized $Co_2MnSi/BTO/SrRuO_3$ MFTJs with a Co_2-TiO_2 termination. The black (red) line represents the majority-spin (minority-spin) DOS. The CBM is indicated by blue circles.

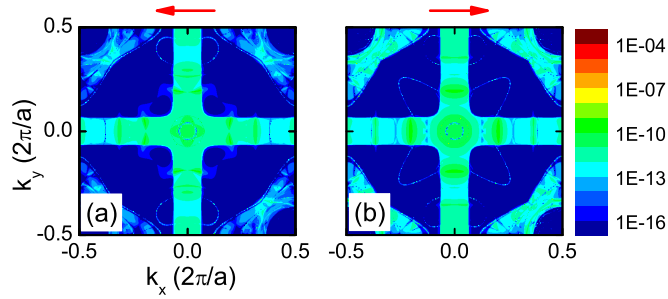

FIG. 9. The $k_{\parallel}$-resolved transmission distributions at the Fermi energy in the 2DBZ for tunnel junctions with a Co_2-TiO_2 termination. Panels (a) and (b) are the left-polarized case and the right-polarized case, respectively.

3. Band edges varying with Ti-O displacement

We vary the Ti-O displacement at the Co_2MnSi-BTO interface from 0.1 to 0.2 Å, and we fix the FE displacements of the other layers. The results are schematically shown in Fig. 10. The band edges of Co_2-TiO_2 [Fig. 10(a)] and MnSi-TiO_2 [Fig. 10(b)] terminated MFTJs show similar variations with the change of local Ti-O displacement. With the increase of interfacial Ti-O displacement (its corresponding polarization direction pointing away from the interface), the band edges in the region where the CBM is higher than the Fermi level move downward gradually, and the tilt of the band edges becomes a little flat, consistent with the description in the main text. In addition, the band edges of the 0.2 Å case in Fig. 10(b) seems different from other cases. Its curved band edges at the Co_2MnSi-BTO interface are like the screening potential at metal interfaces [5]. This is because the band edges near the Co_2MnSi-BTO interface is lower than the Fermi level, and the free electrons in the barrier near the interface directly screen the electrostatic potential drop, resulting in a curved energy band near the interface.

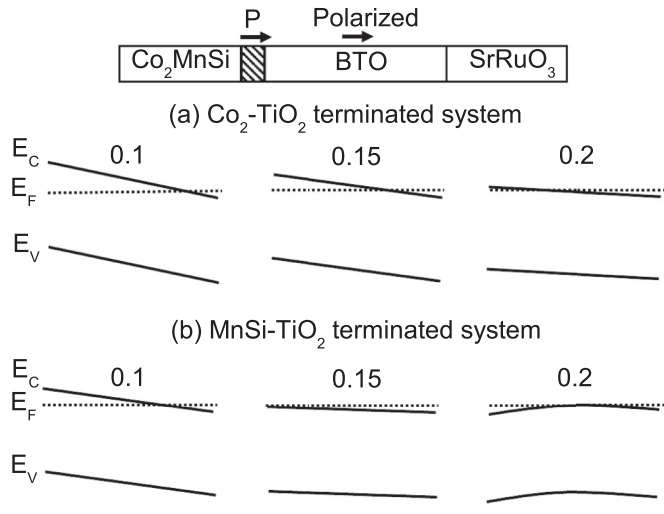

FIG. 10. Schematic of tested band edges for the right-polarized $Co_2MnSi/BTO/SrRuO_3$ MFTJ with (a) a Co_2-TiO_2 termination and (b) a MnSi-TiO_2 termination. Ti-O displacement at the Co_2MnSi-BTO interface marked with shadow is changed between 0.1, 0.15, and 0.2 Å, while other layers of BTO are fixed to 0.2 Å.

[1] J. P. Velev, C. G. Duan, J. D. Burton, A. Smogunov, M. K. Niranjan, E. Tosatti, S. S. Jaswal, and E. Y. Tsymbal, Nano Lett. **9**, 427 (2009).

[2] V. Garcia, M. Bibes, L. Bocher, S. Valencia, F. Kronast, A. Crassous, X. Moya, S. Enouz-Vedrenne, A. Gloter, D. Imhoff, C. Deranlot, N. D. Mathur, S. Fusil, K. Bouzehouane, and A. Barthélémy, Science **327**, 1106 (2010).

[3] D. Pantel, S. Goetze, D. Hesse, and M. Alexe, Nat. Mater. **11**, 289 (2012).

[4] G. Sanchez-Santolino, J. Tornos, D. Hernandez-Martin, J. I. Beltran, C. Munuera, M. Cabero, A. Perez-Muñoz, J. Ricote, F. Mompean, M. Garcia-Hernandez, Z. Sefrioui, C. Leon, S. J. Pennycook, M. C. Muñoz, M. Varela, and J. Santamaria, Nat. Nanotechnol. **12**, 655 (2017).

[5] M. Ye. Zhuravlev, R. F. Sabirianov, S. S. Jaswal, and E. Y. Tsymbal, Phys. Rev. Lett. **94**, 246802 (2005).

[6] N. M. Caffrey, T. Archer, I. Rungger, and S. Sanvito, Phys. Rev. Lett. **109**, 226803 (2012).

[7] M. Ye. Zhuravlev, Y. Wang, S. Maekawa, and E. Y. Tsymbal, Appl. Phys. Lett. **95**, 052902 (2009).

[8] Z. Wen, C. Li, D. Wu, A. D. Li, and N. B. Ming, Nat. Mater. **12**, 617 (2013).

[9] C. Ma, Z. Luo, W. C. Huang, L. T. Zhao, Q. L. Chen, Y. Lin, X. Liu, Z. W. Chen, C. C. Liu, H. Y. Sun, X. Jin, Y. W. Yin, and X. G. Li, Nat. Commun. **11**, 1439 (2020).

[10] L. N. Jiang, Y.-P. Wang, W. Z. Chen, and X. F. Han, Phys. Rev. B **103**, 214441 (2021).

[11] G. Kresse and J. Furthmüller, Phys. Rev. B **54**, 11169 (1996).

[12] J. P. Perdew, A. Ruzsinszky, G. I. Csonka, O. A. Vydrov, G. E. Scuseria, L. A. Constantin, X. Zhou, and K. Burke, Phys. Rev. Lett. **100**, 136406 (2008).

[13] P. E. Blöchl, Phys. Rev. B **50**, 17953 (1994).

[14] G. Kresse and D. Joubert, Phys. Rev. B **59**, 1758 (1999).

[15] J. Taylor, H. Guo, and J. Wang, Phys. Rev. B **63**, 245407 (2001).

[16] Y. J. Shin, Y. Kim, S.-J. Kang, H.-H. Nahm, P. Murugavel, J. R. Kim, M. R. Cho, L. Wang, S. M. Yang, J.-G. Yoon, J.-S. Chung, M. Kim, H. Zhou, S. H. Chang, and T. W. Noh, Adv. Mater. **29**, 1602795 (2017).

[17] K. Yamauchi, B. Sanyal, and S. Picozzi, Appl. Phys. Lett. **91**, 062506 (2007).

[18] L. Y. Chen, C. L. Chen, K. X. Jin, and X. J. Du, Europhys. Lett. **99**, 57008 (2012).

[19] P. K. Rout, H. Pandey, L. Wu, Anupam, P. C. Joshi, Z. Hossain, Y. Zhu, and R. C. Budhani, Phys. Rev. B **89**, 020401(R) (2014).

[20] J. F. Chen, C. S. Lin, Y. Yang, L. Hu, and W. D. Cheng, Modell. Simul. Mater. Sci. Eng. **22**, 015008 (2014).

[21] D. Cao, M.-Q. Cai, W. Y. Hu, and C.-M. Xu, J. Appl. Phys. **109**, 114107 (2011).

[22] M.-Q. Cai, Y. Du, and B.-Y. Huang, Appl. Phys. Lett. **98**, 102907 (2011).

[23] N. Nakagawa, H. Y. Hwang, and D. A. Muller, Nat. Mater. **5**, 204 (2006).

[24] J. M. Rondinelli, N. M. Caffrey, S. Sanvito, and N. A. Spaldin, Phys. Rev. B **78**, 155107 (2008).

[25] L. Chioncel, Y. Sakuraba, E. Arrigoni, M. I. Katsnelson, M. Oogane, Y. Ando, T. Miyazaki, E. Burzo, and A. I. Lichtenstein, Phys. Rev. Lett. **100**, 086402 (2008).

[26] X. Liu, Y. Wang, J. D. Burton, and E. Y. Tsymbal, Phys. Rev. B **88**, 165139 (2013).

[27] K. Momma and F. Izumi, J. Appl. Crystallogr. **44**, 1272 (2011).